International Journal of GEOMATE, March, 2026 Vol.30, Issue 139, pp.1-12
ISSN: 2186-2982 (P), 2186-2990 (O), Japan, DOI: https://doi.org/10.21660/2026.139.5313
Geotechnique, Construction Materials and Environment

INTERACTION EFFECT OF STEEL FIBER AND STIRRUP CONTENT ON THE SHEAR CAPACITY OF HIGH-STRENGTH CONCRETE TRANSFER BEAMS

*Bac An Hoang[1], Phuc Tran Van[1], Nhu Thi Quynh Nguyen[1]

[1]Faculty of Civil Engineering, University of Architecture Ho Chi Minh City, Vietnam;

*Corresponding Author, Received: 28 Oct. 2025, Revised: 27 Dec. 2025, Accepted: 02 Jan. 2026

ABSTRACT: This study investigates the shear behavior and interaction mechanism of high-strength concrete (HSC) transfer beams reinforced with hooked-end steel fibers. The experimental program involved testing large-scale specimens using a four-point bending test setup to simulate the stress conditions in transfer girders. The key investigation parameters included steel fiber contents of 0, 30, and 45 kg/m³ (corresponding to volume fractions of approximately 0%, 0.38%, and 0.57%) and transverse reinforcement ratios (0.15% and 0.30%). The results indicate that steel fibers play a crucial role in the post-cracking behavior by providing a bridging effect across diagonal cracks. This mechanism enhances aggregate interlock and delays the yielding of stirrups, thereby transforming the failure mode from brittle diagonal tension to a more ductile shear-flexure failure. Quantitatively, the inclusion of steel fibers significantly improved the ultimate shear capacity. For the series with 0.15% stirrup ratio, the shear capacity increased from 270 kN (control specimen) to 330 kN (45 kg/m³ fiber content), representing an improvement of approximately 22%. Furthermore, the experimental results were compared with analytical predictions based on ACI 318-19, revealing that the code underestimates the capacity of fiber-reinforced transfer beams by a factor of 2.4 to 3.1, confirming the substantial safety reserve provided by the fiber-stirrup interaction.

Keywords: High-strength concrete, Shear capacity, Steel fiber reinforced concrete (SFRC), Transverse reinforcement, Transfer beam, Crack propagation.

1. INTRODUCTION

In modern multi-story buildings, architectural and functional requirements often necessitate changes in the structural layout between floors. A common challenge arises when the column grid on upper floors does not align with the grid on lower levels, creating a need for large, open spaces for commercial or public use. To address this, transfer beams are widely employed as critical structural elements to redirect heavy loads from the upper columns to the supporting structure below.

By their nature, transfer beams are classified as deep beams, characterized by a large depth-to-span ratio. Unlike conventional slender beams, their behavior is dominated by shear forces rather than flexure, making them susceptible to brittle shear failure, which is sudden and catastrophic [1]. The traditional approach to enhancing shear capacity involves arranging dense stirrups as transverse reinforcement. However, this often leads to steel congestion, which complicates the concrete casting process and can compromise construction quality [2]. This challenge has prompted research into alternative reinforcement methods to enhance concrete properties, particularly through the use of steel fibers [3].

An advanced and effective solution is the use of steel fiber reinforced concrete (SFRC). The uniform dispersion of steel fibers throughout the concrete matrix provides a "bridging" effect across micro-cracks, significantly enhancing the material's tensile strength, ductility, energy absorption capacity, and crack control.

Despite extensive research demonstrating these advantages at the laboratory scale, the practical application of SFRC specifically in large-scale transfer beams within actual building projects appears to remain limited compared to conventional reinforced concrete or prestressed concrete solutions. While SFRC has found successful application in other structural elements like industrial floors, tunnel linings, and certain precast components where its benefits in crack control and durability are well-established, its adoption in critical, heavily loaded transfer structures faces challenges. These may include a lack of specific design provisions in major building codes tailored for SFRC deep beams, perceived higher initial material costs, and potential complexities in quality control during large-volume concrete placement to ensure uniform fiber distribution [4]. Therefore, continued research, particularly focusing on performance under realistic conditions (such as continuity) and interaction with traditional reinforcement, is crucial to building confidence and developing reliable design methodologies that can bridge the gap towards wider practical implementation.

The effectiveness of steel fibers in improving the shear capacity of deep beams has been well-documented in numerous studies worldwide. For instance, pioneering work by Roberts & Ho [5]

demonstrated that fibers could effectively prevent shear failure and enhance ultimate capacity.

Ashour et al. [6] and Mansur & Ong [7] confirmed these benefits for high-strength concrete beams, while more recent studies like Dang et al. [8] and Hamoodi et al. [9] have further quantified the significant improvements in shear strength and deformation characteristics.

However, two significant gaps remain in the existing body of knowledge. First, the vast majority of these investigations have focused on simply supported deep beams, although various techniques to enhance the performance of high-strength concrete structural members have been explored [10]. In practice, transfer beams are often designed as continuous structures, whose behavior under shear is markedly different due to complex moment redistribution and stress concentrations at intermediate supports [11]. Second, while the individual contributions of steel fibers and conventional stirrups are understood, the interaction effect between these two shear-resisting mechanisms has not been thoroughly investigated. It is unclear how the effectiveness of steel fibers changes with varying stirrup ratios, and how this interaction is influenced by the structural configuration (simple vs. continuous).

Therefore, this study aims to address these knowledge gaps through a comprehensive experimental program. The primary objectives are: (1) to analyze the interaction effect between steel fiber dosage and stirrup ratio on the shear behavior of high-strength concrete deep beams; and (2) to directly compare this behavior between simply supported and continuous configurations to provide a more complete understanding for practical design applications.

The remainder of this paper is organized as follows: Section 2 highlights the research significance regarding the interaction mechanism and structural configuration. Section 3 details the experimental program, including material properties, specimen fabrication, and test setup. Section 4 presents the results and comprehensive discussion on failure modes, shear capacity, fiber-stirrup interaction, and comparisons with analytical models. Finally, Section 5 summarizes the key conclusions drawn from the study and proposes recommendations for future research.

2. RESEARCH SIGNIFICANCE

This research offers practical insights for the design of shear-critical SFRC transfer beams, directly supporting the optimization of reinforcement strategies in high-rise construction. By quantifying the interaction between steel fibers and stirrups, the study provides a scientific basis for reducing transverse reinforcement congestion, leading to more constructible and economical solutions without compromising structural safety or ductility. Furthermore, the comparative analysis between simply supported and continuous configurations addresses the realistic behavior of transfer beams in practice. These findings highlight the potential risks of relying solely on simple beam models for complex, statically indeterminate structures, thereby guiding engineers towards more accurate and safe design methodologies for fiber-reinforced deep members.

3. EXPERIMENTAL PROGRAM

To investigate the interaction effects of steel fiber and stirrup content, a comprehensive experimental program was designed and executed. The program involved the fabrication and testing of scaled deep beam specimens, simulating the behavior of actual transfer beams in high-rise buildings at a 1:4 scale.

Although the specimens are scaled down (1:4 scale), the shear span-to-depth ratio ($\boldsymbol{a/d} \approx 1.8$) and reinforcement ratios were chosen to represent the critical shear behavior of full-scale transfer beams. It is acknowledged that larger beams typically exhibit more brittle behavior due to the size effect law; however, the addition of steel fibers is expected to mitigate this effect by bridging micro-cracks and enhancing the fracture process zone, thereby allowing the results to be extrapolated to full-scale members with reasonable confidence.

3.1. Materials

3.1.1. Concrete

Two high-strength concrete (HSC) mixes were designed to achieve target strengths of approximately 40 MPa (Mix 1) and 50 MPa (Mix 2). The constituent materials included Holcim PC40 cement, local river sand, and crushed stone aggregate (maximum size 20-25 mm with continuous grading conforming to ASTM C33 [12] or TCVN 7570:2006 [13] requirements). Tap water and Sika-based superplasticizers were used to ensure workability. The detailed mix proportions are provided in Table 1.

Table 1. Concrete mix proportions

Component	Unit	Mix 1 (Quantity/m³)	Mix 2 (Quantity/m³)
Holcim PC40 Cement	kg	395	552
River sand ($\boldsymbol{M_{d1}}$=2)	kg	673	652
Crushed stone (1x2)	m³	785	784
Water	liters	190	160
Sika admixture	liters	4.0	5.5

Note: Steel fibers were added to these base mixes according to the dosages specified in Table 3.

The mechanical properties were determined through standard testing procedures on 150 mm cubic

specimens: compressive strength was tested in accordance with TCVN 3105:2022 [14], and splitting tensile strength was evaluated according to TCVN 3120:2022 [15]. All average mechanical properties for both mixes are summarized in Table 2.

The workability of the fresh concrete was evaluated using the standard slump test, as specified in ASTM C143 [16]. While the addition of steel fibers typically reduces flowability, in this study, the dosage of the polycarboxylate-based superplasticizer was carefully adjusted for each mix to maintain a consistent consistency suitable for casting large-scale beams. Consequently, the slump values for all batches, including those with fiber contents of 30 and 45 kg/m³, were maintained within the range of 110 to 135 mm. This ensured proper compaction and uniform fiber distribution without segregation.

3.1.2. Reinforcing Steel

The reinforcement system comprised bars (20 mm and 12 mm diameters) for longitudinal reinforcement and plain bars (6 mm diameter) for stirrups. The mechanical properties, including yield strength (f_y) and ultimate strength (f_u), were determined through tensile testing of three samples per bar size in accordance with TCVN 197-1:2014 [17]. These results are listed in Table 2. The modulus of elasticity (E_s) for all steel bars was taken as 200 GPa.

3.1.3. Steel Fibers

Commercially available Dramix® 3D-65/35-BG hooked-end steel fibers were used. These fibers feature a length (L_f) of 35 mm and a diameter (d_f) of 0.55 mm, resulting in an aspect ratio (L_f/d_f) of 64. Their mechanical properties, as provided by the manufacturer, are summarized in Table 2. The fiber dosages were selected based on the recommendations of ACI 544.1R [18] and verified through preliminary trial mixes to ensure adequate workability.

Table 2. Mechanical properties of constituent materials (Mean ± SD)

Material	Property	Unit	Value
Concrete Mix 1	Compressive Strength ($f_{c,cube}$)	Mpa	43.1 ± 2.2
Concrete Mix 2	Compressive Strength ($f_{c,cube}$)	Mpa	58.1 ± 2.3
Main Rebar (d20)	Yield Strength (f_y)	Mpa	516 ± 10
	Ultimate Strength (f_u)	Mpa	639 ± 13
Stirrups (d6)	Yield Strength (f_{yw})	Mpa	317 ± 10
	Ultimate Strength (f_{uw})	Mpa	471 ± 14
Steel Fibers (Dramix 3D)	Tensile Strength (f_f)	Mpa	1345
	Modulus of Elasticity (E_f)	GPa	210

Note: SD = Standard Deviation. The values for concrete and steel reinforcement represent the mean ± SD derived from three standard specimens tested for each batch according to TCVN 3105:2022 (ASTM C39 equivalent) and TCVN 197-1:2014 (ISO 6892-1 equivalent), respectively. Properties of steel fibers are provided by the manufacturer. The splitting tensile strengths (f_{ct}) for Mix 1 and Mix 2 were 4.6 MPa and 5.1 MPa, respectively.

3.2. Specimen Fabrication and Curing

3.2.1. Mixing Procedure

Concrete batches were mixed using a mechanical mixer with a 250-liter capacity. The mixing procedure was carefully controlled to ensure homogeneity and uniform fiber distribution. First, coarse and fine aggregates were dry mixed for approximately 1 minute. Cement was then added, and dry mixing continued for another minute. Subsequently, about 70% of the total water, pre-mixed with the superplasticizer, was added, followed by mixing for 2 minutes.

For SFRC specimens, the steel fibers were manually dispersed into the rotating mixer at a controlled rate over a period of 2–3 minutes to prevent balling. To ensure optimal dispersion, the mixing process was paused briefly for visual inspection to verify that no fiber clumping had occurred before the final water addition.

Finally, the remaining water was added, and mixing continued for an additional 2–3 minutes until a visually uniform and consistent mixture was achieved. Continuous monitoring of the fresh concrete flow during casting confirmed that this rigorous procedure effectively prevented segregation. Furthermore, post-failure examination of the fractured surfaces at various cross-sections served as a qualitative validation, confirming a reasonably uniform fiber distribution throughout the concrete matrix, even at the highest dosage of 45 kg/m³.

3.2.2. Reinforcement Cage and Casting

The reinforcement cages were assembled according to the details shown in Fig. 1. Strain gauges were attached to the designated locations on the longitudinal bars and stirrups before assembly. The cages were then carefully placed into steel formwork, ensuring correct positioning and concrete cover. Concrete was poured into the molds in layers and compacted using handheld immersion vibrators to minimize voids and ensure proper encapsulation of reinforcement and fibers. Along with the beam specimens, cubic specimens (150 mm) were cast from each batch for determining the concrete's mechanical properties.

3.2.3. Curing Regimen

After casting, the specimens were covered with plastic sheeting to prevent moisture loss. The formwork was removed approximately 24 hours after casting. Subsequently, the beams and control cubes were cured under standard laboratory conditions (ambient temperature ranging from 30°C to 35°C and relative humidity around 72-77%). Curing involved keeping the specimens moist (e.g., using wet burlap or regular water spraying) until the day of testing at 28 days. This strict curing was essential to minimize potential shrinkage cracks.

3.3. Test Specimens

A total of 22 beam specimens were fabricated into four groups (A1, A2, B1, and B2). All specimens shared a cross-section of 150 mm x 500 mm. The experimental program investigated four key variables: steel fiber content (m_f: 0, 30, 45 kg/m³), stirrup ratio (ρ_{sw}: 0.15%, 0.30%), concrete strength (f_c: 43.1, 58.1 MPa), and structural configuration (simply supported (Groups A1, A2) vs. two-span continuous (Groups B1, B2). The matrix of the test specimens is presented in Table 3. Reinforcement details and dimensions are illustrated in Fig. 1.

Table 3. Experimental program and specimen matrix

Group	Specimen ID	f_c (MPa)	ρ_{sw} (%)	m_f (kg/m³) [V_f (%)]
A1	D-S-40-00-0.15	43.1	0.15	0 [0%]
A1	D-S-40-30-0.15	43.1	0.15	30 [0.38%]
A1	D-S-40-45-0.15	43.1	0.15	45 [0.57%]
A1	D-S-40-00-0.30	43.1	0.30	0 [0%]
A1	D-S-40-30-0.30	43.1	0.30	30 [0.38%]
A1	D-S-40-45-0.30	43.1	0.30	45 [0.57%]
A2	D-S-50-00-0.15	58.1	0.15	0 [0%]
A2	D-S-50-30-0.15	58.1	0.15	30 [0.38%]
A2	D-S-50-45-0.15	58.1	0.15	45 [0.57%]
A2	D-S-50-00-0.30	58.1	0.30	0 [0%]
A2	D-S-50-30-0.30	58.1	0.30	30 [0.38%]
A2	D-S-50-45-0.30	58.1	0.30	45 [0.57%]
B1	D-C-40-00-0.15	43.1	0.15	0 [0%]
B1	D-C-40-30-0.15	43.1	0.15	30 [0.38%]
B1	D-C-40-45-0.15	43.1	0.15	45 [0.57%]
B1	D-C-40-00-0.30	43.1	0.30	0 [0%]
B1	D-C-40-30-0.30	43.1	0.30	30 [0.38%]
B2	D-C-50-00-0.15	58.1	0.15	0 [0%]
B2	D-C-50-30-0.15	58.1	0.15	30 [0.38%]
B2	D-C-50-45-0.15	58.1	0.15	45 [0.57%]
B2	D-C-50-00-0.30	58.1	0.30	0 [0%]
B2	D-C-50-30-0.30	58.1	0.30	30 [0.38%]

3.4. Test Setup and Instrumentation

All tests were conducted at the Structural Engineering Laboratory of the Ho Chi Minh City University of Technology [19].

Loading: The load was applied using a hydraulic jack through a steel spreader beam to ensure uniform stress distribution. The load was applied quasi-statically to observe the cracking behavior at each stage, with the loading rate controlled by displacement at approximately 0.5 mm/minute. For simply supported beams, a single concentrated load was applied at mid-span, while for two-span continuous beams, loads were applied simultaneously at the mid-point of each span. The load was increased incrementally until the specimen reached its peak load-bearing capacity, followed by a significant drop in load, signifying the complete structural failure.

Instrumentation: Data was recorded using a TDS-303 Data Logger. Linear Variable Differential Transformers (LVDTs) were used to measure beam deflections at the supports and mid-span. To monitor the behavior of the reinforcement, electrical resistance strain gauges were attached directly to the longitudinal bars and stirrups at critical locations (mid-span and near supports) to accurately capture the yielding evolution. Additionally, the width of cracks was measured at each load step using a specialized crack-width microscope with a reading precision of 0.02 mm. The overall test setup and instrumentation layout are illustrated in Fig. 2. To demonstrate the data acquisition process and reliability, a representative set of raw time-series data for a typical SFRC specimen is provided in Table A1 (Appendix).

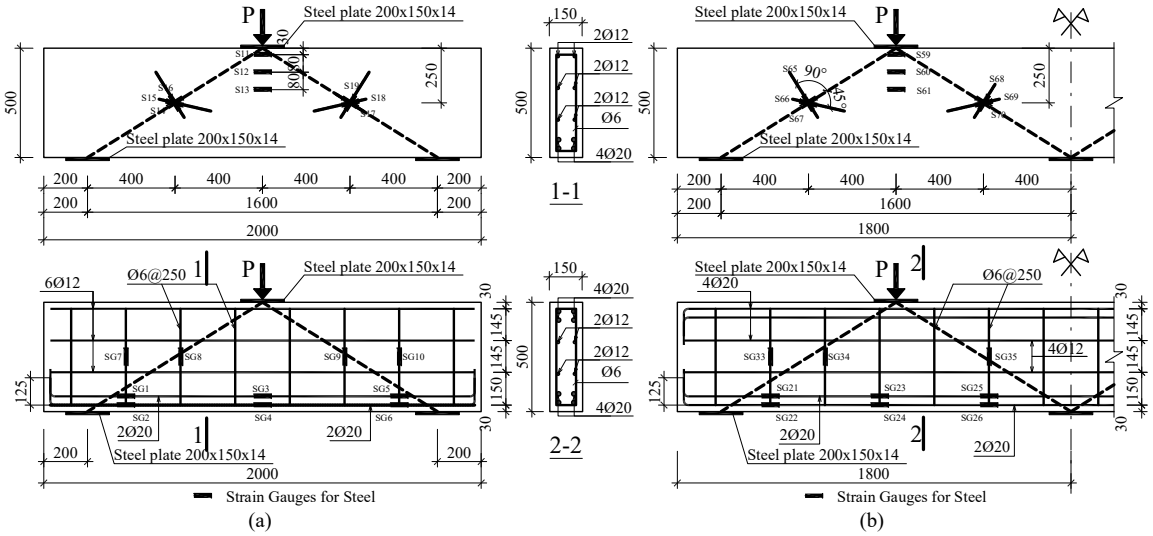

Fig. 1. Specimen dimensions and reinforcement details: (a) Simply supported beams; (b) Two-span continuous beams

(a)

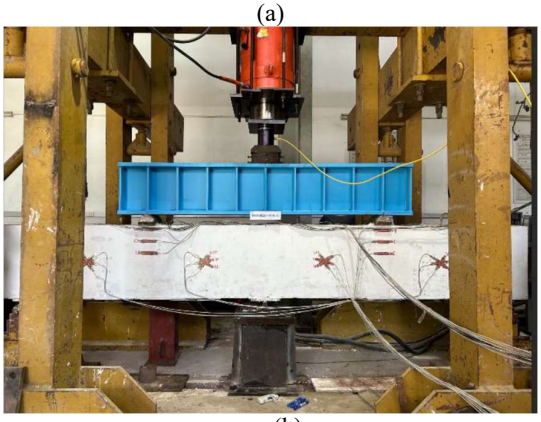

(b)

Fig. 2. Test setup and instrumentation: (a) Simply supported beams; (b) Two-span continuous beams

4. RESULTS AND DISCUSSION

4.1. Failure Modes and Cracking Patterns

The failure process across all tested specimens exhibited a consistent sequence. Flexural cracks typically initiated at mid-span around 13-17% of the ultimate load ($\boldsymbol{P_u}$), followed by the formation of diagonal shear cracks at approximately 30-35% $\boldsymbol{P_u}$, indicating a transition to shear-dominated behavior. However, the presence of steel fibers introduced a significant difference in the post-cracking response. Control specimens (without fibers) displayed characteristic brittle shear failure, involving the rapid propagation of a single, dominant diagonal crack leading to abrupt failure, which is typical for shear-critical deep beams [1].

In contrast, fiber-reinforced specimens demonstrated a more ductile failure mode. The steel fibers provided a "bridging effect" across crack surfaces, effectively distributing stresses and arresting the propagation of the primary diagonal crack. This resulted in a system of multiple, finer, and more evenly distributed diagonal cracks, a well-documented phenomenon in SFRC behavior [5, 7]. Quantitatively, when compared at the same absolute load level before failure, the crack widths in the fiber-reinforced beams were significantly smaller than those in the control specimens, with a reduction of up to 83%. This difference is clearly illustrated in Fig. 3.

Furthermore, the crack mapping analysis revealed a significant difference in crack spacing. The control beams exhibited sparse major cracks with an average spacing of approximately 180–250 mm. In contrast, the SFRC beams showed a denser network of micro-cracks with a reduced average spacing of 40–70 mm, confirming the enhanced stress redistribution capability of the fiber-matrix interaction.

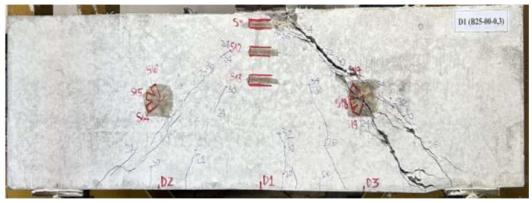

(a)

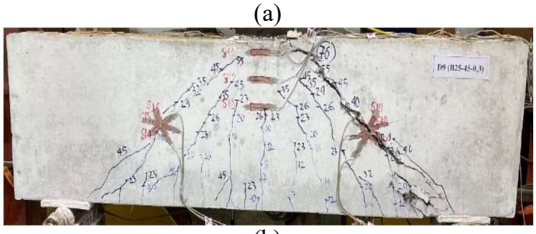

(b)

Fig. 3. Typical failure modes: (a) Control beam (D-S-40-00-0.15); (b) SFRC beam (D-S-40-45-0.30)

In summary, the observed cracking patterns and failure modes qualitatively confirm the beneficial role of steel fibers. Their inclusion transitioned the inherently brittle shear failure typical of control deep beams towards a more ductile response, characterized by a distributed system of finer cracks rather than a single dominant failure plane. This visual evidence underscores the effectiveness of the fiber bridging mechanism in enhancing post-cracking performance.

4.2. Analysis of the Behavior of Simply Supported Beams (Groups A1 & A2)

4.2.1 Load-Displacement Relationship and Shear Capacity

The load-displacement responses for the simply supported beam groups are presented in Fig. 4. These curves clearly show that while the initial stiffness was similar among specimens, those reinforced with steel fibers maintained significantly higher post-cracking stiffness compared to the control beams. Consequently, displacements at equivalent load levels were reduced, with reductions ranging from 17.9% to 21.6% observed at the ultimate load capacity of the corresponding control specimens. Data summarized in Table 3 and Fig. 5 confirm that both the inclusion of steel fibers and an increase in the stirrup ratio markedly improved the diagonal

cracking load ($P_{cr,sh}$) and, crucially, the ultimate shear capacity (P_u). The addition of 45 kg/m³ of steel fibers increased the ultimate shear capacity by up to 25.0%, as detailed in Table 4.

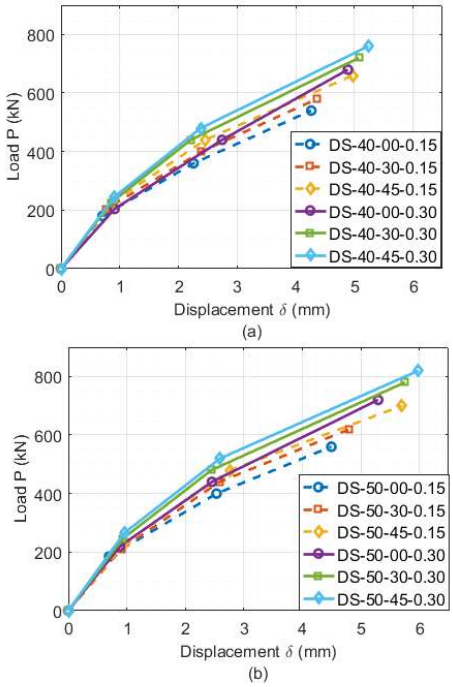

Fig. 4. Load-displacement relationship for simply supported beams: (a) Groups A1 (f_c = 43.1 MPa) ; (b) Groups A2 (f_c = 58.1 MPa).

Table 4. Key experimental results for simply supported beams (Groups A1 & A2)

Specimen ID	ρ_{sw} (%)	m_f (kg/m³) [V_f (%)]	$P_{cr,sh}$ (kN)	P_u (kN)	Increase in P_u (%)*
Group A1 (f_c=43,1 MPa)					
D-S-40-00-0.15	0.15	0 [0%]	180	540	-
D-S-40-30-0.15	0.15	30 [0.38%]	203	580	7.4
D-S-40-45-0.15	0.15	45 [0.57%]	226	660	22.2
D-S-40-00-0.30	0.3	0 [0%]	204	680	-
D-S-40-30-0.30	0.3	30 [0.38%]	225	720	5.9
D-S-40-45-0.30	0.3	45 [0.57%]	244	760	11.8
Group A2 (f_c=58,1 MPa)					
D-S-50-00-0.15	0.15	0 [0%]	185	560	-
D-S-50-30-0.15	0.15	30 [0.38%]	210	620	10.7
D-S-50-45-0.15	0.15	45 [0.57%]	235	700	25
D-S-50-00-0.30	0.3	0 [0%]	220	720	-
D-S-50-30-0.30	0.3	30 [0.38%]	245	780	8.3
D-S-50-45-0.30	0.3	45 [0.57%]	265	820	13.9

Note: The increase in P_u (%) is calculated by comparing with the control specimen (without steel fibers) within the same stirrup ratio (ρ_{sw}) and concrete strength group. Values presented are from single large-scale specimen tests corresponding to each parameter configuration. Due to the large scale and complexity of the transfer beam specimens, statistical variation (Mean ± SD) is not applicable here, unlike the material property tests. Strict fabrication controls were implemented to minimize experimental variability.

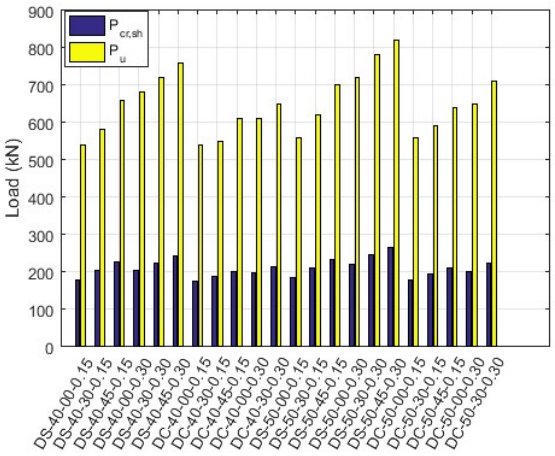

Fig. 5. Comparison of shear cracking ($P_{cr,sh}$) and ultimate (P_u) loads for all specimens

4.2.2. Interaction between Steel Fibers and Stirrups

A deeper analysis of the results presented in Table 3 reveals a distinct interaction between the effects of steel fibers and stirrups. The enhancement in ultimate shear capacity provided by steel fibers was more pronounced at the lower stirrup ratio (ρ_{sw} = 0.15%), compared to the higher ratio (ρ_{sw} = 0.30%). For instance, in Group A2, the capacity increase dropped from 25.0% to 13.9% when the stirrup ratio was doubled.

To understand this interaction mechanism, the stirrup strain data, presented in Fig. 6, were examined. While stirrup strains were negligible before diagonal cracking, they increased rapidly afterward, indicating the stirrups' active role in shear resistance. Crucially, Fig. 6 shows that steel fibers significantly reduced stirrup strains at equivalent load levels and delayed the onset of yielding. Specifically, at the ultimate load of a control beam, the stirrup strain in the equivalent fiber-reinforced beam (45 kg/m³) could be reduced by as much as 84.3%. This quantitative evidence supports the hypothesis that steel fibers effectively redistribute shear stresses within the cross-section; the fiber-concrete matrix carries a portion of the shear force, thereby reducing the demand on the stirrups and delaying their yielding. Similar to findings by Onyelowe et al. [20] regarding the optimization of constituent interactions in high-performance concrete, the load transfer path in this study is significantly improved by the bridging effect of steel fibers. This mechanism effectively redistributes the internal stresses across the diagonal cracks, thereby delaying the degradation of aggregate interlock and enhancing the overall shear resistance. This confirms that the contributions of fibers and stirrups are not simply additive and suggests opportunities for optimizing reinforcement design by partially substituting stirrups with fibers to enhance ductility and constructability.

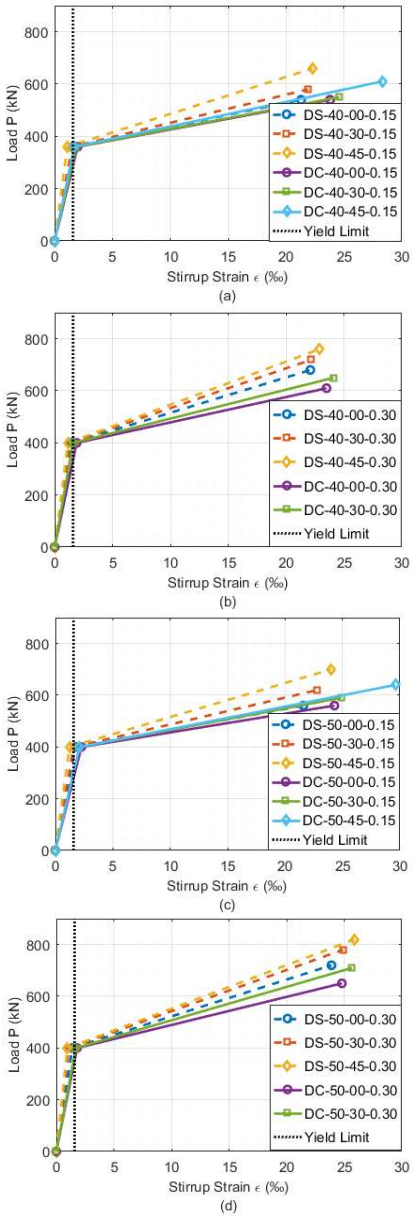

Note: The vertical dotted line indicates the yield displacement.

Fig. 6. Load versus stirrup strain relationships: (a) f_c =43.1 MPa, ρ_{sw} =0.15% ; (b) f_c =43.1 MPa, ρ_{sw} =0.30%; (c) f_c =58.1 MPa, ρ_{sw} =0.15%; (d) f_c=58.1 MPa, ρ_{sw}=0.30%

4.2.3. Energy Absorption Capacity

To evaluate the influence of steel fibers on structural ductility, the Energy Absorption Capacity (EAC) was calculated as the area under the load-displacement curves shown in Fig. 4, representing the total work done until failure [21]. The EAC results for the simply supported beams, summarized in Table 5, demonstrate a clear trend: the addition of steel fibers substantially increased the energy absorption capacity, indicating enhanced overall ductility. This effect was particularly significant in the higher-strength concrete group (A2), where specimen D-S-50-45-0.15 exhibited a 61.3% increase in EAC compared to its control counterpart. This provides strong evidence for the role of steel fibers in promoting a more ductile failure mode, especially in high-strength concrete.

Table 5. Energy Absorption Capacity (EAC) for simply supported beams (Groups A1 & A2)

Specimen ID	ρ_{sw} (%)	m_f (kg/m³) [V_f (%)]	EAC (kNm)	Increase in EAC (%)*
Group A1 (f_c=43,1 MPa)				
D-S-40-00-0.15	0.15	0 [0%]	1.410	-
D-S-40-30-0.15	0.15	30 [0.38%]	1.588	12.6
D-S-40-45-0.15	0.15	45 [0.57%]	2.075	47.2
D-S-40-00-0.30	0.30	0 [0%]	1.937	–
D-S-40-30-0.30	0.30	30 [0.38%]	2.297	18.6
D-S-40-45-0.30	0.30	45 [0.57%]	2.508	29.5
Group A2 (f_c=58,1 MPa)				
D-S-50-00-0.15	0.15	0 [0%]	1.593	-
D-S-50-30-0.15	0.15	30 [0.38%]	1.886	18.4
D-S-50-45-0.15	0.15	45 [0.57%]	2.569	61.3
D-S-50-00-0.30	0.30	0 [0%]	2.352	–
D-S-50-30-0.30	0.30	30 [0.38%]	2.869	22.0
D-S-50-45-0.30	0.30	45 [0.57%]	3.174	34.9

Note: The increase in EAC (%) is calculated by comparing with the control specimen (without steel fibers) within the same stirrup ratio (ρ_{sw}) and concrete strength group. Values presented are from single large-scale specimen tests corresponding to each parameter configuration. Due to the large scale and complexity of the transfer beam specimens, statistical variation (Mean ± SD) is not applicable here, unlike the material property tests. Strict fabrication controls were implemented to minimize experimental variability.

In essence, the detailed analysis of simply supported beams provided clear quantitative evidence of the interaction between steel fibers and stirrups. While both components enhance shear capacity and ductility (measured via EAC), their combined effect is not purely additive, with fiber effectiveness diminishing at higher stirrup ratios. Crucially, the stirrup strain data demonstrated that fibers actively redistribute shear stresses, delaying stirrup yielding and providing a mechanistic explanation for the observed interaction.

4.3. Comparative Analysis with Continuous Beams

Comparing the results with the continuous beam specimens (Groups B1 & B2), which better simulate actual transfer beam conditions, reveals significant behavioral differences and, critically, a reduction in the effectiveness of steel fibers compared to the simply supported configuration.

4.3.1. Comparison of Load-Bearing Capacity and Deformation

Continuous beams consistently exhibited lower load-bearing capacities than their simply supported counterparts.

Table 6. Key experimental results for continuous beams (Groups B1 & B2)

Specimen ID	ρ_{sw} (%)	m_f (kg/m³) [V_f (%)]	$P_{cr,sh}$ (kN)	P_u (kN)	Increase in P_u (%)*
Group B1 (f_c = 43.1 MPa)					
D-C-40-00-0.15	0.15	0 [0%]	175	540	-
D-C-40-30-0.15	0.15	30 [0.38%]	189	550	1.9
D-C-40-45-0.15	0.15	45 [0.57%]	201	610	13.0
D-C-40-00-0.30	0.30	0 [0%]	198	610	-
D-C-40-30-0.30	0.30	30 [0.38%]	215	650	6.6
Group B2 (f_c = 58.1 MPa)					
D-C-50-00-0.15	0.15	0 [0%]	180	560	-
D-C-50-30-0.15	0.15	30 [0.38%]	195	590	5.4
D-C-50-45-0.15	0.15	45 [0.57%]	210	640	14.3
D-C-50-00-0.30	0.30	0 [0%]	200	650	-
D-C-50-30-0.30	0.30	30 [0.38%]	225	710	9.2

Note: The increase in P_u (%) is calculated by comparing with the control specimen (without steel fibers) within the same stirrup ratio (ρ_{sw}) and concrete strength group.

As detailed in Table 6, both the diagonal cracking load ($P_{cr,sh}$) and the ultimate shear capacity (P_u) were reduced, with P_u showing decreases of up to 9.7% for comparable specimens (Table 7, Fig. 7). This reduction is likely due to the complex stress redistribution inherent in statically indeterminate structures. More pronounced differences were observed in deformation and crack control. Continuous beams experienced substantially larger crack widths (up to 3.7 times wider) and higher stirrup strains (up to 2.7 times higher) at similar load stages compared to simple beams. This can be attributed to the negative moments at intermediate supports inducing top flexural cracks that interact complexly with diagonal shear cracks. This intricate crack pattern compromises the fiber bridging mechanism's effectiveness compared to the more uniform crack field in simple beams, consistent with observations in other studies on continuous deep beams [11,22]. The resulting reduced stiffness and heightened stress concentrations contribute to premature failure at lower capacities.

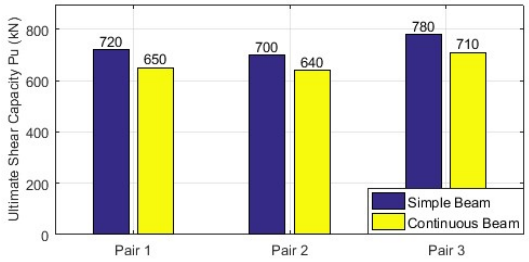

Fig. 7. Comparison of ultimate shear capacity (P_u) between corresponding simple and continuous beams (Pairs defined in Table 7).

Table 7. Comparison of key results between corresponding simple and continuous beams

Comparison Pair	Specimen ID	Shear Capacity, P_u (kN)	Crack Width, w_u (mm)	Stirrup Strain, $\epsilon_{su,stirr}$ (‰)
Pair 1 (f_c=43.1 MPa, ρ_{sw}=0.30%, m_f=30)	D-S-40-30-0.30	720	3.14	22.18
	D-C-40-30-0.30	650 (-9.7%)	3.32 (+5.7%)	24.14 (+8.8%)
Pair 2 (f_c=58.1 MPa, ρ_{sw}=0.15%, m_f=45)	D-S-50-45-0.15	700	3.70	24.01
	D-C-50-45-0.15	640 (-8.6%)	3.85 (+4.1%)	29.66 (+23.5%)
Pair 3 (f_c=58.1 MPa, ρ_{sw}=0.30%, m_f=30)	D-S-50-30-0.30	780	3.80	24.94
	D-C-50-30-0.30	710 (-9.0%)	3.93 (+3.4%)	25.68 (+3.0%)

Note: Values in parentheses indicate the percentage change of the continuous beam relative to the corresponding simple beam.

4.3.2. Comparison of Steel Fiber Effectiveness and Energy Absorption

A key finding is the significantly diminished effectiveness of steel fibers in enhancing the structural performance of continuous beams compared to simple beams. This phenomenon can be attributed to the complex stress redistribution in statically indeterminate structures, where the interaction between high shear forces and negative bending moments at the intermediate support creates a severe multi-axial stress state that limits the efficiency of fiber bridging.

Table 8. Energy Absorption Capacity (EAC) for continuous beams (Groups B1 & B2)

Specimen ID	ρ_{sw} (%)	m_f (kg/m³) [V_f (%)]	EAC (kNm)	Increase in EAC (%)*
Group B1 (f_c = 43.1 MPa)				
D-C-40-00-0.15	0.15	0 [0%]	964	-
D-C-40-30-0.15	0.15	30 [0.38%]	1.023	6.1
D-C-40-45-0.15	0.15	45 [0.57%]	1.190	23.4
D-C-40-00-0.30	0.30	0 [0%]	1.221	–
D-C-40-30-0.30	0.30	30 [0.38%]	1.263	3.4
Group B2 (f_c = 58.1 MPa)				
D-C-50-00-0.15	0.15	0 [0%]	1.115	-
D-C-50-30-0.15	0.15	30 [0.38%]	1.202	7.8
D-C-50-45-0.15	0.15	45 [0.57%]	1.492	33.8
D-C-50-00-0.30	0.30	0 [0%]	1.444	–
D-C-50-30-0.30	0.30	30 [0.38%]	1.610	11.5

Note: The increase in EAC (%) is calculated by comparing with the control specimen (without steel fibers) within the same stirrup ratio (ρ_{sw}) and concrete strength group.

The percentage increase in ultimate shear capacity (P_u) achieved by adding fibers was markedly lower for continuous beams (max 14.3%) compared to simple beams (max 25.0%), as illustrated in Fig. 8.

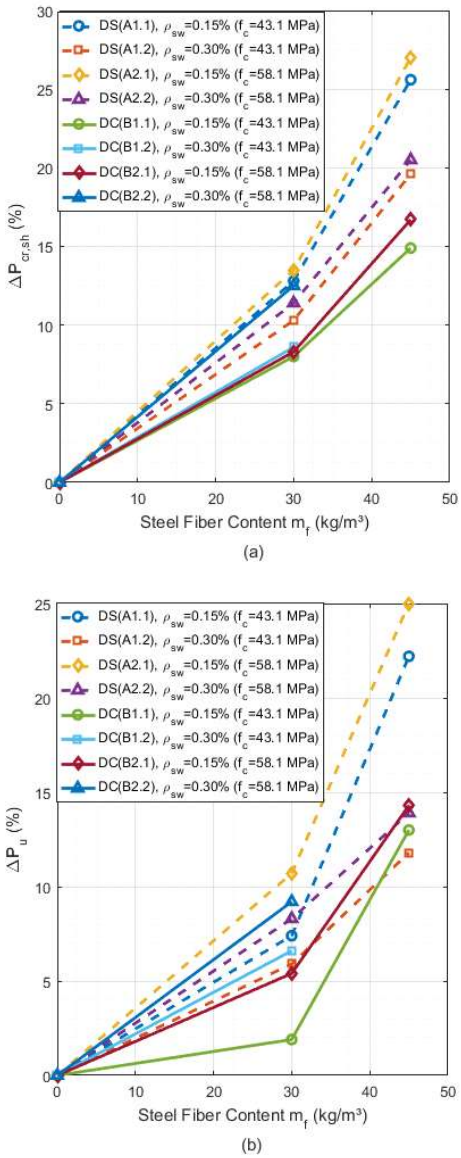

Fig. 8. Percentage increase in load capacity vs. steel fiber content: (a) Shear cracking load ($\Delta P_{cr,sh}$); (b) Ultimate load (ΔP_u)

This reduced effectiveness is even more apparent in the energy absorption capacity (EAC), summarized in Table 8. While EAC in simple beams increased by up to 61.3%, the maximum increase for continuous beams was limited to 33.8% (Fig. 9). These results quantitatively demonstrate that the statically indeterminate nature of continuous beams curtails the beneficial effects of steel fibers [23]. The complex moment redistribution and combined stress states likely limit the full mobilization of the fiber bridging mechanism, which performs better in the more uniform shear zones of simply supported beams. This underscores the need for caution when extrapolating SFRC benefits observed in simple beam tests to continuous structures.

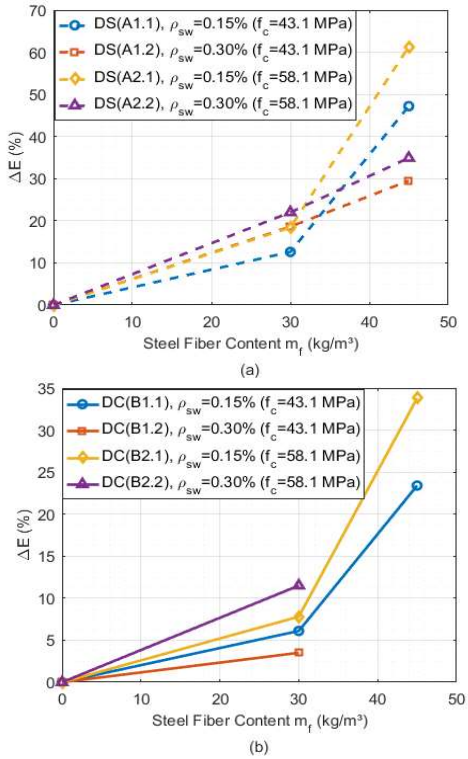

Fig. 9. Percentage increase in Energy Absorption Capacity (ΔE) vs. steel fiber content: (a) Simple beam groups; (b) Continuous beam groups

In conclusion, the comparative analysis strongly highlights the significant influence of structural configuration on SFRC deep beam behavior. Continuous beams consistently demonstrated lower shear capacities and exhibited larger deformations and crack widths compared to their simply supported counterparts. Most importantly, the effectiveness of steel fibers in enhancing shear capacity, controlling cracks, and improving energy absorption was markedly reduced under conditions of continuity. This underscores the critical need for caution when extrapolating findings from simple beam tests to the design of continuous transfer structures commonly found in practice.

4.4. Comparison with Analytical Models

To evaluate the structural safety margin provided by the addition of steel fibers, the experimental ultimate shear capacities ($\boldsymbol{V_{exp}}$) of the simply supported beams (Groups A1 & A2) were compared with the analytical predictions ($\boldsymbol{V_{ACI}}$) calculated based on ACI 318-19 [1]. The nominal shear strength provided by ACI 318 considers the contribution of concrete ($\boldsymbol{V_c}$) and stirrups ($\boldsymbol{V_s}$) based on the actual material properties and beam dimensions (b=150 mm, d=438 mm), but it disregards the contribution of steel fibers. The comparison results are summarized in Table 9.

Table 9. Comparison between experimental and predicted shear capacities

Specimen ID	f'_c (MPa)	Stirrup Ratio (%)	V_{exp} (kN)	V_{ACI} (kN)	Ratio (V_{exp}/V_{ACI})
Group 1: Mix M40 (ρ_{sw}=0.15%)					
D-S-40-00-0.15	43.1	0.15	270.0	104.6	2.58
D-S-40-30-0.15	43.1	0.15	290.0	104.6	2.77
D-S-40-45-0.15	43.1	0.15	330.0	104.6	3.16
Group 2: Mix M40 (ρ_{sw}=0.30%)					
D-S-40-00-0.30	43.1	0.30	340.0	135.8	2.50
D-S-40-30-0.30	43.1	0.30	360.0	135.8	2.65
D-S-40-45-0.30	43.1	0.30	380.0	135.8	2.80
Group 3: Mix M50 (ρ_{sw}=0.15%)					
D-S-50-00-0.15	58.1	0.15	280.0	116.4	2.41
D-S-50-30-0.15	58.1	0.15	300.0	116.4	2.58
D-S-50-45-0.15	58.1	0.15	340.0	116.4	2.92
Group 4: Mix M50 (ρ_{sw}=0.30%)					
D-S-50-00-0.30	58.1	0.30	360.0	147.6	2.44
D-S-50-30-0.30	58.1	0.30	380.0	147.6	2.57
D-S-50-45-0.30	58.1	0.30	400.0	147.6	2.71

As shown in Table 9, all tested beams exhibited a safety ratio ($\boldsymbol{V_{exp}}$ / $\boldsymbol{V_{ACI}}$) significantly greater than 1.0, ranging from 2.41 to 3.16. Even the control beams without fibers showed a ratio greater than 2.0, which can be attributed to the arch action mechanism typical in shear-critical transfer beams ($\boldsymbol{a/d \approx 1.8}$) that standard beam-shear equations tend to underestimate.

Significantly, the inclusion of steel fibers enhanced this safety ratio by approximately 15-20% compared to the control specimens. This enhancement confirms that the ACI 318 code predictions are conservative for HSC transfer beams and that steel fibers provide a substantial reserve of shear capacity by bridging cracks and maintaining aggregate interlock—mechanisms that are not currently accounted for in the standard code provisions for shear reinforcement.

5. CONCLUSIONS

Based on the experimental investigation of high-strength concrete transfer beams reinforced with steel fibers and stirrups, the following conclusions are drawn:

1. **Shear Capacity Enhancement**: The inclusion of hooked-end steel fibers significantly improved the ultimate shear capacity of the transfer beams. Specifically, adding 45 kg/m³ (V_f = 0.57%) of steel fibers increased the shear capacity by up to 25.0% compared to the control beams. The improvement was most effective in specimens with lower stirrup ratios (ρ_{sw} = 0.15%), confirming the efficiency of fibers in reducing reinforcement congestion.
2. **Ductility and Failure Mode**: Steel fibers transformed the failure mode from brittle diagonal tension to a more ductile shear-flexure failure. The Energy Absorption Capacity (EAC) was enhanced significantly, with the highest increase of 61.3% observed in the M50 mix series. The fibers effectively bridged diagonal cracks, maintaining post-cracking stiffness and structural integrity.
3. **Fiber-Stirrup Interaction**: Quantitative analysis of strain data revealed a beneficial interaction mechanism. At equivalent load levels, the presence of steel fibers reduced the strain in stirrups by up to 84.3%, significantly delaying the onset of stirrup yielding. This confirms that fibers actively participate in carrying shear stresses, relieving the demand on transverse reinforcement.
4. **Comparison with Design Codes**: A comparison with ACI 318-19 predictions showed that current code provisions are conservative for SFRC transfer beams. The experimental-to-predicted shear capacity ratio (V_{exp}/V_{ACI}) ranged from 2.41 to 3.16. This substantial safety margin (approximately 15-20% higher than control beams) suggests that an empirical factor accounting for fiber contribution could be introduced in future design guidelines to optimize material usage.
5. **Future Studies**: Based on the current findings, future research should focus on the behavior of SFRC transfer beams under cyclic loading to evaluate seismic performance. Additionally, developing finite element numerical models to conduct extensive parametric studies on different shear span-to-depth ratios (a/d) and hybrid fiber combinations is recommended to broaden the applicability of the proposed solution.

6. ACKNOWLEDGEMENTS

The authors gratefully acknowledge the support of the Ministry of Construction (MOC), the University of Architecture Ho Chi Minh City, and the Structural Engineering Laboratory at Ho Chi Minh City University of Technology for the research project titled "Investigation on the Load-Bearing Capacity and Deformation of Transfer Beam Structures in High-Rise Buildings Using High-Strength Concrete and Steel Fiber Reinforced High-Strength Concrete," grant number RD 34-22.

7. REFERENCES

1. ACI Committee 318, Building Code Requirements for Structural Concrete (ACI 318-19) and Commentary, American Concrete Institute, Farmington Hills, MI, USA, 2019,

pp. 1–628.
2. Yoo D.Y., Yang J.M., Effects of stirrup, steel fiber, and beam size on shear behavior of high-strength concrete beams, Cement and Concrete Composites, Vol. 87, 2018, pp. 137–148. DOI:10.1016/j.cemconcomp.2017.12.010.
3. Amalia S.Y., Tiyani L., Murdiyoto A., Effect of Rice Husk Ash and Steel Fibers on Self-Compacting Concrete Properties, International Journal of GEOMATE, Vol. 25, No. 108, 2023, pp. 130-137. DOI:10.21660/2023.108.3677.
4. Amin M.N., Ahmad W., Khan K., Ahmad A., Steel Fiber-Reinforced Concrete: A Systematic Review of the Research Progress and Knowledge Mapping, Materials, Vol. 15, No. 17, 2022, Art. no. 6155. DOI: 10.3390/ma15176155.
5. Roberts T.M., Ho N.L., Shear failure of deep fibre reinforced concrete beams, International Journal of Cement Composites and Lightweight Concrete, Vol. 4, No. 3, 1982, pp. 145–152. DOI:10.1016/0262-5075(82)90040-9
6. Ashour S.A., Wafa F.F., Shear Behavior of High-Strength Fiber Reinforced Concrete Beams, ACI Structural Journal, Vol. 89, No. 2, 1992, pp. 176-184.
7. Mansur M.A., Ong K.C.G., Behavior of Reinforced Fiber Concrete Deep Beams in Shear, ACI Structural Journal, Vol. 88, No. 1, 1991, pp. 98–105. DOI: 10.14359/3128
8. Dang T.D., Tran D.T., Nguyen-Minh L., Nassif A.Y., Shear resistant capacity of steel fibres reinforced concrete deep beams: An experimental investigation and a new prediction model, Structures, Vol. 33, 2021, pp. 2284–2300. DOI: 10.1016/j.istruc.2021.05.091.
9. Hamoodi A.Z., Zewair M.S., Ojaimi M.F., Shear Behavior of Fiber-Reinforced Concrete Beams: An Experimental Study, International Journal of GEOMATE, Vol. 21, No. 86, 2021, pp. 167–179. DOI:10.21660/2021.86.j2263.
10. Mauludin L.M., Permana R., Ruslan U., Zulpanani A., Fauziah L., Nurhayati S.M., Savira M.G., Enhancing Performance of High-Strength Concrete Using Bacillus Megaterium as Self-Healing Agent, International Journal of GEOMATE, Vol. 26, No. 114, 2024, pp. 68-75. DOI:10.21660/2024.114.4290.
11. Ashour A.F., Tests of Reinforced Concrete Continuous Deep Beams, ACI Structural Journal, Vol. 94, No. 1, 1997, pp. 3–12.
12. ASTM C33/C33M, Standard specification for concrete aggregates, ASTM International, West Conshohocken, PA, USA, 2018, pp. 1–8.
13. TCVN 7570:2006, Aggregates for concrete and mortar - Specifications, Ministry of Science and Technology, Hanoi, Vietnam, 2006, pp. 1-11.
14. TCVN 3105:2022, Fresh and hardened concrete - Sampling, making and curing of test specimens, Ministry of Science and Technology, Vietnam, 2022, pp. 1-17.
15. TCVN 3120:2022, Hardened concrete – Test method for splitting tensile strength, Ministry of Science and Technology, Vietnam, 2022, pp. 1-8.
16. ASTM C143/C143M, Standard test method for slump of hydraulic-cement concrete, ASTM International, West Conshohocken, PA, USA, 2020, pp. 1-4.
17. TCVN 197-1:2014, Metallic materials - Tensile testing - Part 1: Method of test at room temperature, Ministry of Science and Technology, Vietnam, 2014, pp. 1-62.
18. ACI Committee 544. (1996). ACI 544.1R-96: Report on Fiber Reinforced Concrete (Reapproved 2009), ACI, USA, pp. 1-66.
19. Tran V.P., Nguyen M.L., Hoang B.A., Phan T.L., Nguyen T.Q.N., Research on the bearing capacity and deformation of transfer beam structures for high-rise buildings using high-strength concrete and high-strength concrete reinforced with dispersed steel fibers, Ministry-Level Research Project, No. RD 34-22, Ho Chi Minh City, 2024, pp. 1-156.
20. Onyelowe K.C., Hanandeh S., Ulloa N., Barba-Vera R., Moghal A.A.B., Ebid A.M., Arunachalam K. P., Ur R.A., Developing machine learning frameworks to predict mechanical properties of ultra-high performance concrete mixed with various industrial byproducts, Scientific Reports, Vol. 15, No. 1, 2025, Art. no. 24791. DOI: 10.1038/s41598-025-08780-y.
21. Park R., Evaluation of ductility of structures and structural assemblages from laboratory testing, Bulletin of the New Zealand Society for Earthquake Engineering, Vol. 22, No. 3, 1989, pp. 155–166. DOI:10.5459/bnzsee.22.3.155-166
22. Zhang N., Tan K.H., Direct strut-and-tie model for single span and continuous deep beams, Engineering Structures, Vol. 29, No. 11, 2007, pp. 2987–3001. DOI:10.1016/j.engstruct.2007.02.004
23. Nhu N.T.Q., Tuyen T.N.L., Long N.M., An H.B., Le P.T., Phuc T.V., Experimental analysis of shear behavior of continuous and simple steel fiber reinforced concrete deep beams, Journal of Science and Technology in Civil Engineering (STCE) - HUCE, Vol. 19, No. 2, 2025. DOI: 10.31814/stce.huce2025-19(2V)-03.

APPENDIX

Table A1. Representative raw test data for Specimen D-S-50-45-0.15 (Data Excerpt) (Selected data points representing key behavior stages: elastic, cracking, yielding, and ultimate)

Time (s)	Load P (kN)	Mid-span Deflection δ (mm)	Stirrup Strain $\boldsymbol{\varepsilon_{sw}}$ ($\boldsymbol{\mu\varepsilon}$)	Max Crack Width $\boldsymbol{w_{max}}$ (mm)	Remarks
0	0.0	0.00	0	0.00	Start
120	50.4	0.24	12	0.00	Elastic
240	100.8	0.49	28	0.00	Elastic
360	151.2	0.76	45	0.00	Elastic
485	235.0	1.21	185	0.05	Shear Cracking ($\boldsymbol{P_{cr,sh}}$)
600	300.5	1.65	320	0.08	Fiber Bridging Active

Appendix Table A1 continue

840	400.2	2.45	650	0.12	Service Load Range
1080	500.6	3.38	1120	0.25	Crack Propagation
1320	600.4	4.42	1850	0.65	Pre-peak
1450	650.1	4.95	2240	1.10	Stirrup Yielding
1580	700.0	5.62	3150	2.85	Ultimate Load ($\boldsymbol{P_u}$)
1620	630.5	6.80	5400	>3.00	Post-peak / Failure

Note: Data was recorded using a TDS-303 Data Logger with a sampling rate of 1 Hz. Strain data ($\boldsymbol{\varepsilon_{sw}}$) represents the gauge located at the critical shear span. The table displays extracted steps to illustrate the load history; the full dataset contains over 1,800 data points.